REVISION 2 – correction date August 8, 2014

Cathodoluminescence dependence on feldspar mineral structure and implications for forensic geology

Sarah A. Brokus[1,2a], Danielle K. Silletti[1,2b], J. Mark Lunderberg[2c], Paul A. DeYoung[3], Graham F. Peaslee[1,2], Dyanne E. Carpenter[1d], and JoAnn Buscaglia[4]

[1]FBI Laboratory, Visiting Scientist Program, Counterterrorism and Forensic Science Research Unit, Quantico, VA 22135, U.S.A.
[2]Hope College, Chemistry Department, Holland, MI 49423, U.S.A.
[3]Hope College, Physics Department, Holland, MI 49423, U.S.A.
[4]FBI Laboratory, Counterterrorism and Forensic Science Research Unit, Quantico, VA 22135, U.S.A.
[a]Present address: Northern Illinois University, Geology Department, DeKalb, IL 60115, U.S.A.
[b]Present address: Loyola University Chicago, Burn and Shock Trauma Research Institute, Maywood, IL 60153, U.S.A.
[c]Present address: University of Chicago, Chicago, IL 60637, U.S.A.
[d]Present address: FBI Laboratory, Latent Print Operations Unit, Quantico, VA 22135, U.S.A.

ABSTRACT

A collection of 42 feldspar mineral samples from a wide geographical range of North America was examined by cold-cathode cathodoluminescence (CL) spectroscopy. Characteristic wavelength peaks, which were determined to be independent of geographic origin, were associated with each feldspar phase. Most of these peaks were attributed to previously assigned Mn^{2+} and Fe^{3+} luminescent centers and structural defects. An unattributed set of infrared (IR) peaks was observed in many samples; one uncommon ultraviolet (UV) peak was observed in samples from two locations. The peak centroids associated with the Mn^{2+} and Fe^{3+} luminescent centers vary with stoichiometric changes in the K-Na-Ca composition of the feldspars. For both alkali and plagioclase feldspars, shifts in CL peak centroids correlate well with lattice size, as measured by x-ray diffraction (XRD). Additional analyses of the feldspar samples by electron microprobe analysis (EMP), particle-induced x-ray emission spectroscopy (PIXE), energy-dispersive micro-X-ray fluorescence spectroscopy (μXRF), and/or laser-ablation inductively

coupled plasma mass spectrometry (LA-ICP-MS) were conducted for confirmation of elemental composition. These results demonstrate the potential of CL spectroscopy, a relatively nondestructive analytical technique, to facilitate rapid discrimination between feldspar samples. The addition of CL spectroscopy of feldspars to existing forensic analytical protocols for geologic materials has the potential to provide support for casework, both to discriminate sources in a forensic comparison, as well as to constrain the provenance of an unknown sample.

Keywords: Luminescence, feldspar, forensic geology, spectroscopy

INTRODUCTION

Mineral luminescence can occur when electrons excited by the passage of ionizing radiation relax and release photons. Luminescence is only possible when the deposited energy of the incident radiation is sufficient to allow electrons to jump the band gap of a crystal lattice. Specific trace elements as well as lattice defects within the mineral's crystal structure create intermediate energy levels between valence bands and conduction bands for additional electron transitions, allowing certain minerals to luminesce brightly at specific wavelengths in the ultraviolet, visible, and near infrared (UV-vis-NIR) regions following irradiation (Götze et al. 2000; Götze 2002). Although these electronic transitions occur at specific wavelengths, interactions with non-shielding electrons produce broad peaks typical of a cathodoluminescence (CL) spectrum (Götze 2000; Götze 2002). The peak centroids of these transitions are dependent on the crystal field experienced by the luminescent center and on the chemical composition of the mineral (Krbetschek et al. 2002).

Although the mechanisms that give rise to mineral luminescence are widely known, most CL experimental studies remain qualitative in nature because the relative peak intensity within samples is highly variable. This variability of luminescence intensities has been attributed to many factors, including instrumental/analytical factors (e.g., incident radiation intensity variation, (Thomas 1987)), crystal-chemical factors (e.g., defect/element concentration (Götze et al. 1999; Haberman 2002; Parsons et al. 2008), sensitizing, quenching (Kabler 1964), etc.), and interactions between the solid and the incident electron beam (e.g., orientation angle dependence of the crystalline sample with respect to the ion beam (Walderhaug and Rykkje 2000; Finch et al. 2003; Munisso et al. 2007; Garcia-Guinea et al. 2007)). Recently, a quantitative use of CL peak centroid wavelengths has been proposed as a forensic method to identify minerals and characterize the mineral chemistry of geological trace evidence (Palenik and Buscaglia 2007). The study reported in this paper describes the reproducibility of CL spectra from feldspar samples and the forensic utility of geographical source attribution using CL signatures from commonly encountered feldspar minerals.

Feldspars are found ubiquitously on the earth's crust; therefore, techniques that specifically determine feldspar provenance may be important tools in future forensic investigations (Ruffell and McKinley 2005; Pye and Blott 2009). Geographic provenance of geological samples has utility in forensic science when dealing with intelligence and criminal matters. For the purposes of this study, we define provenance to be the geological origin of the mineral, rather than a purely forensic science definition. CL microspectrophotometry may make it possible to rapidly analyze sediment samples and characterize the bulk mineral chemistry of large numbers of

diverse feldspar minerals based on their CL spectrum. Although CL peak intensities vary dramatically even between mineral grains of the same phase within a source, CL peak centroids remain constant within a homogenous sample because they result from the crystal field experienced by the luminescent centers within the mineral (i.e., mineral structure). For CL data to be utilized forensically, the within-source variability should be small relative to the between-source variability. That is, (1) similar minerals from the same location should yield similar CL spectral peak positions and (2) similar minerals from different locations should yield CL spectra with different peak centroids. If the CL peak centroids vary by geographic location, just as mineral formations vary, then these data could provide insight about the provenance of a sample. Cold-cathode CL spectroscopy could then be used to quickly show distinctive characteristics of the feldspars within each sample. The purpose of this particular study is to demonstrate the potential for CL measurements of any particular feldspar sample to yield reproducible peak centroids that vary significantly in different geographical regions of North America. This is a necessary first step with museum-quality samples required to show that such a technique could be used to distinguish feldspar provenance. Although further studies will be necessary to demonstrate that feldspar crystals of one rock complex are homogeneous enough to provide useful information for forensic geological investigations, this initial study demonstrates that this method could be a viable forensic tool.

METHODS

Forty-two feldspar samples, including 20 alkali feldspars (referring to any feldspar with the general formula $K[AlSi_3O_8]$) and 22 plagioclase feldspars (referring to any feldspars of the general formula $(Na,Ca)[Al(Si,Al)Si_2O_8]$), of known provenance were obtained from the

Department of Mineral Sciences of the Smithsonian Institution National Museum of Natural History and Ward's Science. The provenance of the feldspar samples encompasses a broad geographic area of North America and the samples include a range of feldspar types from well-characterized geological formations. The lithological unit that describes each formation from which feldspar samples were collected was identified in Bernard and Hyršl (2004); details of these samples and their locations are listed in Appendix 1.

Each mineral sample was mechanically fractured into fragments ~300-700 μm in diameter and each fragment was evaluated visually using reflected light (RL) stereomicroscopy. Specimens were excluded if the inner surfaces of the fragments exhibited extensive weathering or any sort of visual impurity, such as the mixture of two visible minerals. Because RL microscopy does not provide a complete sample characterization, homogeneity of every sample is not guaranteed; however, obvious heterogeneous fragments were excluded from our analyses.

From each fractured feldspar sample, six replicate crystal fragments were analyzed with CL, followed by ion-beam induced luminescence (IBIL). After the luminescence spectra were obtained by CL and IBIL analysis to demonstrate the variety of luminescent signatures available across the sample set, the elemental composition of these grains was determined by energy-dispersive micro-X-ray fluorescence (μXRF) spectroscopy. The major and minor chemical element composition of each feldspar sample was confirmed using energy-dispersive micro-X-ray fluorescence spectroscopy (μXRF), using the same grains that were nondestructively studied by CL and IBIL. Some of the feldspar samples, although not the same grains on which CL and IBIL were obtained, were also analyzed using electron microprobe analysis (EMP) and particle-

induced X-ray emission (PIXE) spectroscopy to confirm the characterization by μXRF. An additional replicate fragment of each feldspar sample was analyzed with minimal destruction using laser-ablation inductively coupled plasma mass spectrometry (LA-ICP-MS) to investigate the presence of trace elements of interest using a more sensitive analytical method. Additional replicates were also selected and mechanically ground into a fine powder for measurement by X-ray diffraction (XRD) for crystallographic information.

Spectrometer wavelength calibration was verified for the luminescence spectral analysis techniques (CL and IBIL) using a sample of zircon that was obtained from the John P. Wehrenberg reference collection (Montana State University, Missoula, MT); this zircon sample was chosen because of the numerous rare-earth element lines with narrow peak widths across its CL spectrum.

All luminescence spectra collected had background baselines subtracted to minimize the effect of background light noise. Because the relatively broad luminescence peaks observed are not Gaussian in wavelength space, the background-subtracted luminescence spectra were converted to energy space, deconvolved and fit with 4-6 peaks using the commercial software, OriginLab® (http://www.originlab.com) and converted back to wavelength space.

CL

Six replicate hand-selected mineral grains from each of the 42 feldspar and 1 zircon mineral samples were mounted on double-sided, spectroscopic-grade carbon tape adhered to aluminum slides. Excitation was conducted *in vacuo* using a CITL MK 5-2 cold-cathode CL system with an

accelerating voltage of ~11.6 kV, a current of ~400 μA, and a beam spot size of approximately 1 cm^2. The cold-cathode CL vacuum stage with a leaded glass optical window was centered under a Leica S8 APO stereomicroscope with a 10X objective. Spectroscopic measurements in the range of 350-1050 nm were made using a fiber-optic cable attached to an Ocean Optics USB4000 spectrometer fit to the dual-port stereomicroscope; the entire spectral region was measured at one time for each replicate measurement. Typical acquisition times for the spectroscopic measurements were 1-16 s. Blank backgrounds were manually subtracted offline using the OriginLab® software for each spectrum. All CL spectral data reported in this paper were collected with this system.

Interlaboratory analyses were conducted using a second CL system. For the purposes of this paper, the data acquired using this second CL system are included solely for the discussion of the wavelength dependence of detection efficiency for cold-cathode instrumentation in general and the implications for forensic science applications. The second CL system, a cold-cathode Luminoscope ELM-3R CL system, was used for sample excitation *in vacuo*, with an accelerating voltage of 10 kV and a current of 1 mA. The electron beam was focused onto the sample using permanent magnets for a beam spot size of approximately 0.3 cm^2. The cold-cathode CL vacuum stage with a leaded glass optical window was centered under a Nikon Eclipse E800 polarized light microscope with a 10X extra-long working distance objective. Spectroscopic measurements in the range of 300-1100 nm were made using a fiber-optic cable attached to a Horiba Jobin-Yvon TRIAX 320 spectrometer, with a 1 mm slit width, a 1200 groove/mm grating, and a Horiba Jobin-Yvon Symphony® CCD detector. Two 2.5-s acquisitions at each wavelength were obtained from each sample and averaged to give a final spectrum; the entire spectral region was

measured at one time for each replicate measurement. Blank backgrounds were subtracted in SynerJY™ (Horiba Jobin-Yvon) software upon collection.

IBIL

The six feldspar samples from Ward's Science and one zircon calibration sample were exposed to a 3.4 MeV proton beam produced at the Hope Ion Beam Analysis Laboratory; for each analysis, the exact same mineral grains as those analyzed by the CITL-MK 5-2 cold-cathode CL system were used. IBIL measurements used low beam currents of ~1 nA and micro-focused beam spots of ~50 μm diameter to prevent sample degradation. For all sample analyses, the spot size was smaller than the target mineral grains and multiple locations per grain were sampled. Spectroscopic measurements in the range of 350-1050 nm were made using light collected from a lens mounted at ~145° to the beam and ~2 cm from the target via a fiber-optic cable attached to an Ocean Optics USB4000 spectrometer (the same spectrometer as used for the CITL-CL measurements). The entire spectral region was measured at one time for each replicate measurement. Blank backgrounds of the target were subtracted offline using the PeakFit®4.0 software for Windows to account for the effect of background light noise.

μXRF

The elemental compositions of the same six replicates of 42 individual mineral grains that were analyzed by CL and IBIL were determined using μXRF. A Horiba XGT-7000V X-ray microscope with a rhodium excitation source, 400 μm monocapillary, and a liquid nitrogen-cooled, high-purity Si detector was used to acquire the μXRF spectra. An accelerating voltage of 30 kV was used, and the X-ray tube current was auto-adjusted for optimum dead time; each

spectrum was acquired for 1200 live seconds. The samples were measured in two orientations relative to the excitation beam in order to distinguish interfering diffraction peaks from characteristic X-ray emission peaks. An external soda-lime silica glass standard reference material, NIST SRM 1831 (National Institute for Standards and Technology, Gaithersburg MD) was analyzed multiple times with each analytical run as a system performance check and used as a single-point calibration standard.

XRD

One separate subsample of each mineral sample was ground into a fine powder, which was placed on a mono-crystalline-silicon, zero-background sample holder, and analyzed using a PANalytical X'Pert Pro diffractometer. Analysis conditions included: a nickel filter, 0.04 radian Soller slits, a fixed divergence slit (0.25°), 0.08° step size, 1 deg/s, 16 spins/min, and a 2θ range of 5-75°. The commercial software program, X'Pert HighScore version 2.2e (2.2.5, release date 02-03-2009, PANalytical B.V. 2003) was used to evaluate the data; data were searched using several International Centre for Diffraction Data databases, including PDF-2 (2008), PDF-4+ with SIeve+ (2010), and the Joint Committee on Powder Diffraction Standards' PDF cards (Berry 1974).

LA-ICP-MS

Direct solid sampling of one additional replicate mineral grain from each feldspar sample (other than those grains on which CL, IBIL, and μXRF measurements were made) was carried out using a New Wave Research UP-213 Nd:YAG 213 nm laser ablation system. Ablation was conducted using helium gas flow through the sample cell, with argon make-up carrier gas. The

laser conditions were: 70% power, pulse frequency of 20 Hz, and a 160 μm spot size. Three replicate 90-s ablation spots were acquired per feldspar grain. For each ablation, a background signal was collected for 32 seconds, 30 seconds of which were integrated for background correction to allow for slight inconsistencies in the manual start of mass spectral data acquisition. The ablated material was analyzed with a Hewlett-Packard 4500plus quadrupole ICP-MS; 60 seconds of signal during ablation were integrated per isotope. Data for the following isotopes were acquired: ^{23}Na, ^{25}Mg, ^{27}Al, ^{29}Si, ^{39}K, ^{42}Ca, ^{49}Ti, ^{57}Fe, ^{85}Rb, ^{88}Sr, ^{90}Zr, ^{137}Ba, ^{138}Ba, ^{139}La, ^{140}Ce, ^{146}Nd, ^{153}Eu, and $^{206, 207, 208}$Pb. To correct for instrument drift over long analytical runs, an external glass standard reference material NIST SRM 612 (National Institute of Standards and Technology, Gaithersburg, MD) and a sample of reference glass FGS1 (Latkoczy et al. 2005) were analyzed multiple times within each run.

PIXE

The same mineral grains analyzed by CL and IBIL were also analyzed by PIXE spectroscopy. X-rays were detected in a lithium-drifted silicon detector mounted at 145° to the beam of 3.4 MeV protons that were focused to a ~50 μm spot on multiple locations within each mineral grain. Approximately 1-2 nA of beam was delivered for 600 s for a total charge deposition of approximately 0.5-1 μC. The beam current was integrated before and after each run with a Faraday cup and an absolute normalization was obtained from backscattered protons detected in a surface barrier silicon detector at 168° to the beam. The X-ray spectra were analyzed using a thick-target option in GUPIXWin software (Maxwell et al. 1995). A solid-target NIST SRM 2586 standard was used to normalize the absolute elemental concentrations.

241 **EMP**

242 Feldspar reference samples obtained from Ward's Science were analyzed with the University of
243 Georgia Department of Geology's JEOL 8600 EMP using a 15 kV accelerating voltage and 5 or
244 10 nA beam currents. Quantitative analyses were performed with a wavelength dispersive
245 spectrometer (WDS) automated with Geller Microanalytical Laboratory's dQANT software,
246 using 10-s counting times, and both natural and synthetic mineral standards (Smithsonian
247 Microbeam Standards, http://mineralsciences.si.edu/facilities/standards.htm#1). Analyses were
248 calculated using Armstrong's (1988) Phi-Rho-Z matrix correction model. Backscattered electron
249 photomicrographs were acquired using Geller Microanalytical Laboratory's dPICT imaging
250 software. A 10 μm diameter beam was used when possible, but exsolution lamella in some of the
251 samples necessitated using 1 or 5 μm beam diameters.
252
253
254 **RESULTS AND DISCUSSION**
255
256 **Elemental composition**
257 The elemental compositions obtained via μXRF are plotted on a traditional feldspar ternary
258 diagram (Fig. 1) and are tabulated in Appendix 1. The μXRF data were selected for presentation
259 in Fig. 1 because they were acquired from the same particles as those measured with CL and
260 IBIL, thereby permitting direct comparison of the spectroscopic results to the elemental
261 composition.
262

To confirm the μXRF characterization of the samples, the elemental composition obtained by more penetrating probe techniques (PIXE and EMP) on replicate samples were compared to the μXRF results. An example of this comparison is shown in Fig. 2 for the calcium content in five feldspar samples obtained from Ward's Science. There is good agreement between all three elemental characterization techniques for all but the bytownite sample, which suggests that the incident beam penetration depth (~70-100 μm for μXRF) was sufficient for bulk analysis of the samples and accurately represents the percent orthoclase, anorthite, and albite composition for each sample.

Despite our careful selection using RL stereomicroscopy, in which we attempted to choose only highly homogeneous samples, most feldspars exhibit some sample microheterogeneity. Due to this mineral sample heterogeneity and the microsampling of the LA method, higher variability in the calculated elemental concentrations was noted for some grains with LA-ICP-MS than with μXRF. In addition to the different sensitivities of the two methods, some of the differences between the results calculated with LA-ICP-MS and μXRF are likely due to the fact that the same feldspar grains displaying microheterogeneity were not analyzed with both techniques. Further, variations in and differences between elemental analyses may also be caused by zoning in the feldspar grains.

Peak assignment

Representative luminescence spectra obtained from CL and IBIL spectroscopy are shown in Fig. 3. Each of the peaks is labeled with its respective luminescence source.

From literature references (Götze et al. 2000; Krbetschek et al. 2002; Gorobets and Rogojine 2002) and independent elemental analysis, it was observed that most of the characteristic luminescent signatures could be ascribed to four sources: (1) Al-O* lattice defect peak centered around 450 nm, (2) Si-O* lattice defect peak centered around 500 nm, (3) Mn^{2+} ions for the peak centered at 540-620 nm, and (4) Fe^{3+} ions for the peak centered at ~680-750 nm. Two additional peaks were required to fit certain samples, including: (5) a peak around 410 nm most likely attributable to Cu^{2+} (Hofmeister and Rossman 1985; Johnston et al. 1992) and (6) a triplet peak between 850-950 nm, possibly attributable to Pb^{+} (Nagli and Dyachenko 1988; Fockele et al. 1989; Erfurt 2003; Erfurt and Krbetschek 2003). Si-O* and Al-O* defect peak centroids have consistent wavelengths between samples, whereas peaks resulting from Fe^{3+} and Mn^{2+} reflect the mineral's structure; the positions of the peak centroids shift and is dependent on the surrounding crystal lattice.

Reproducibility

For these feldspar samples, which are not heavily weathered and have no major impurities, CL peak centroids were consistent within minerals of the same composition (Fig. 3). These results illustrate the homogeneity of the samples and the reproducibility of the peak centroid positions observed for any feldspar hand samples in this study. However, using cold-cathode CL, spectral peak intensities varied greatly both within replicates of a single sample and between different feldspar samples with similar mineral composition. External influences, sample orientation with respect to the electron beam, electron beam intensity, or electron channeling, make reproducible quantification of luminescence intensity of a peak in a sample impossible for this technique. However, quantitative measurements can be made for each of the observed peak centroid values.

These values may be associated with separate mineral crystal structures that vary by location because they were formed under different conditions. The variety found in geological formations, based on their geographical location, is reflected through the feldspar sample's CL spectra, which are distinct from one another.

Provenance distinction

When CL spectra from feldspars of similar mineral composition from different geographical locations were compared, there were notable variations resulting from the diversity of trace elemental compositions**,** lattice sizes, and structures. This is shown for a subset of samples in Fig. 4. The peak centroids corresponding to the spectra shown in Fig. 4 are listed in Table 1. Although several of the primary spectral features are similar within feldspars of a certain chemical composition, each of the samples measured in this study were distinguishable from all of the others by the CL peak centroids when they originated from different geological formations. This suggests that these spectral features could be used to suggest or constrain provenance given a sufficient library of known mineral luminescence spectra.

Whereas the luminescence peak intensity is too variable to be used quantitatively, the luminescence peak wavelength reflects the crystal field gradient that surrounds the *d*-orbitals of the luminescent centers within the mineral. As the lattice size changes due to differences in trace element composition or lattice defects, the observed peak energies change as well, allowing specific signatures for each mineral to be measured and compared (Mora and Ramseyer 1992). Replicate measurements on the same sample show remarkable reproducibility for the luminescence peak centroids, whereas measurements of samples from different geographic

331 locations show significant variability in the measured spectrum. This variability allowed for
332 complete discrimination of the samples in this limited study.
333
334 **Relation to crystal structure**
335 The red and near-IR feldspar CL peaks are due to trace Fe^{3+} ions, known to substitute for the T1
336 and T2 Al^{3+} tetrahedral coordination sites within the alkali feldspar structure (Deer et al. 1966;
337 Telfer and Walker 1978; Finch and Klein 1999). The centroid of this Fe^{3+} peak has been
338 previously observed to experience a hypsochromic shift in CL (Krbetschek et al. 2002) as a
339 function of chemical composition. Krbetschek et al. (2002) suggests the CL peak's
340 hypsochromic shift is due to the substitution of the larger K^+ ion for the smaller Na^+ ion in the
341 mineral as the %Ab increases until %Ab reaches 50%, but Krbetschek et al. (2002) does not
342 confirm this conclusion with any XRD data. The crystal lattice changes dimension with
343 chemical composition changes (Ribbe 1975), presumably resulting in a change in the crystal
344 field experienced by the luminescent center. To test this hypothesis, our study measured the
345 lattice d-spacing values directly by XRD. The d-spacing values representing a given plane (002)
346 were compared to CL Fe^{3+} peak centroids in Fig. 5. As shown in this figure, both the alkali and
347 Ca-rich plagioclase feldspar peak centroids reflect the effect of elemental substitution on
348 structural parameters within the lattice. This feature, therefore, defines the Fe^{3+} CL signature.
349 There is also a strong correlation between the peak centroid position and Ca content in
350 plagioclase and Ca-rich plagioclases, and K content in potassium feldspars. The Fe^{3+} peak
351 intensity varied widely between samples and only those spectra with a Fe^{3+} peak exceeding 10%
352 of the total spectral area were included in this analysis. Peaks with smaller areas have greater
353 uncertainties in their centroid locations and were, therefore, omitted from this analysis.

In Fig. 5, Ca-rich plagioclase was observed to exhibit a trend opposite of the alkali feldspar, presumably because the complexity of the substitution within the plagioclase structure alters the crystal field experienced by Fe^{3+} in a different manner. This could also be explained by the use of the plane perpendicular to the c-axis of the crystal, known to exhibit a different length and ordering in the plagioclase and alkali feldspar. However, when comparing the increase in calcium with the peak position of Fe^{3+} in our data set (data not shown), we do observe the same trend reported by Krbetschek et al. (2002). It is important to note that the Si-O* and Al-O* lattice defect peaks, as well as the Na-rich (greater than 50% Albite) feldspar samples, do not exhibit any peak shift in CL with change in lattice dimension.

Variation with excitation source and detection efficiency

It is interesting to note that some peak centroid wavelengths do not reproduce reported peak centroids from similar feldspars in hot-cathode CL studies or peak centroids observed in studies that used different luminescent techniques (Rendell and Clark 1997; Correcher and Garcia-Guinea 2001; Krbetschek et al. 2002). For example, the observed peak centroids for Fe^{3+} range between 670 and 725 nm in this work, whereas another study has reported peak centroids for Fe^{3+} that range between 700 and 740 nm (Krbetschek et al. 2002). This lack of reproducibility could be due to the different feldspar samples studied, but our technique comparison (CL vs. IBIL) as well as our interlaboratory CL comparison suggests that this could also be due to the differences in excitation source for the luminescence, as well as significant detection efficiency effects for the spectrometers involved. The variability due to the source of sample excitation was confirmed by measuring an individual feldspar grain sample with CL and then measuring the same grain using IBIL spectroscopy, and as described in the methods section, both

377 measurements were made with the same spectrometer. For some geological samples, consistency
378 between CL and IBIL peak centroid wavelengths was demonstrated with replicate spectra of the
379 same mineral sample. For example, the peak centroid wavelengths of the CL and IBIL spectra
380 from zircon grains shown in Fig. 6 are indistinguishable. These zircon samples luminesce
381 following irradiation because of the rare earth element (REE) luminescent center (Dy^{3+}), which
382 produces narrow bands due to highly shielded electronic transitions resulting in limited ranges of
383 excitation (orbitals *f-f* and *f-d*) (Götze 2000). Although considerably more light is produced with
384 IBIL than with cold-cathode CL, the peak positions of both the REEs and the silicate matrix are
385 indistinguishable between the two techniques (Fig. 6). However, in the feldspar samples
386 analyzed in this study, although the lattice defect peak positions were consistent for all feldspars,
387 there were observable bathochromic- and hypsochromic-shifts, primarily in the peaks
388 attributable to Fe^{3+} and the unattributed IR peak (Fig. 7), but also in the peaks ascribed to Cu^{2+}.
389
390 The peak at ~400 nm, which is likely a result of Cu^{2+} luminescent centers (based on PIXE
391 elemental analysis and literature analyses of feldspars from Oregon), also exhibited a peak shift
392 between IBIL and CL spectra. Comparing CL and IBIL spectra collected on the same sample,
393 there is no peak centroid shift observed for the Mn^{2+} peak, the Fe^{3+} IBIL peak centroid shows a
394 bathochromic shift relative to its CL position, and the Cu^{2+} IBIL peak centroid shows a
395 hypsochromic shift relative to its CL position.
396
397 A possible explanation for this shift in peak centroid wavelength could be in *d*-orbital changes
398 resulting from light-induced electron spin state trapping (LIESST) (Gütlich et al. 1994); LIESST
399 could be altering the *d*-orbital configuration of the luminescence centers within the minerals.

Further study is needed to elucidate the mechanism for this shift as a function of luminescence technique. However, in conducting an interlaboratory comparison of cold-cathode CL instrumentation, a significant bathochromic shift was observed for broad CL peaks in the range of 600-750 nm when identical samples were analyzed with the Horiba Jobin-Yvon spectrometer (which is more sensitive in this spectral region) compared to the Ocean Optics spectrometer. For the narrow calibration wavelengths of REEs or fluorescent source standards, this shift was not observed, but for the typical Fe^{3+} luminescence that spans over 100 nm in range, there was an observed shift of ~20 nm. The significantly different detection efficiency of the respective spectrometers (Palenik and Buscaglia 2007) in this wavelength range undoubtedly shift the relative intensity detected within a Fe^{3+} luminescence peak, causing the Ocean Optics system to report peak centroids ~20 nm lower than the Horiba Jobin-Yvon spectrometer. Although the CL results are encouraging for the practical application of feldspar identification and provenance attribution, it is important to note that a single instrument should be used to compare samples unless the detection efficiency is well characterized and normalized. The IBIL results from the same mineral grains indicate that some peak centroids that result from luminescent centers may also be sensitive to the ionizing radiation used, again suggesting limits on comparisons made between different excitation sources.

Unattributed IR peak

Many of the spectra include an unattributed IR peak (~840-950 nm). The IR peak was present in a greater number of samples analyzed using the CL system with the Horiba Jobin-Yvon spectrometer, and many of these peaks were not detected using the CL system with the Ocean Optics spectrometer, presumably due to the IR detection efficiency of the respective

423 spectrometers. Preliminary trace elemental analysis using LA-ICP-MS was performed on many
424 of these feldspar samples to determine if this IR peak could be attributed to the presence of a
425 trace element. For the six samples with an IR peak reported in Appendix 1 (F1, F5, F10, F11,
426 F17 and F18), the average Pb concentration was measured to be above 570 ppb. For all the rest
427 of the samples measured (N=26, except F13), the average Pb concentration was measured to be
428 below 30 ppb. The only notable anomaly is F13, which has a very high Pb content (~3700 ppb)
429 but no detectable IR peak in the CL spectra from any of its replicates. These data suggest the
430 presence of Pb in those samples with the largest IR peaks, whereas most of the samples with no
431 detectable IR peaks also had no detectable levels of Pb. Alkali feldspars are known to have high
432 trace Pb concentrations (Deer et al. 1966), and Pb emission lines have been reported in this
433 wavelength region (Reader et al. 1980; Ralchenko et al. 2011).
434
435 **IMPLICATIONS**
436 There is significant forensic potential for luminescence spectroscopy of common minerals such
437 as feldspars. Whereas the luminescence peak intensity is too variable to be used quantitatively,
438 the luminescence peak position reflects the composition and size of the crystal field gradient that
439 surrounds the *d*-orbitals of the luminescent centers within the mineral. As the lattice size
440 changes, the observed peak energies change as well, which allows specific signatures for each
441 mineral to be measured and compared. The CL spectra change with different feldspar
442 chemistries, allowing most feldspars to be distinguished from other feldspars based on the CL
443 colors they emit. These CL spectral differences could facilitate rapid discrimination between
444 feldspars using a relatively nondestructive analytical technique: CL spectroscopy. Because it is
445 both rapid and nondestructive, CL spectroscopy can be easily incorporated into existing forensic

446 analytical protocols for geologic materials, without additional risk of damage or loss of evidence,
447 which may occur with some traditional chemical methods.
448
449 The forensic examination of sediment can provide both investigative information to support an
450 ongoing criminal investigation and evidence for presentation in court. Casework typically
451 consists of the comparison of a sediment sample of unknown origin (e.g., a sediment sample
452 recovered from the tire or wheel well of a suspect's vehicle) with one of known source (e.g.,
453 sediment from a specific crime scene location); evaluation of a sediment sample of unknown
454 source for provenance determination can also provide valuable support in investigations. The
455 interested reader is referred to Pye and Croft (2004) and Morgan and Bull (2007) for a general
456 overview of forensic sediment analysis, and to Petraco, Kubic and Petraco (2008) and Bowen
457 and Caven (2013) for specific examples of forensic case studies and forensic provenance
458 investigations. The addition of CL spectroscopy of feldspars to these published methods has the
459 potential to provide support for casework, both to discriminate sources in a forensic comparison,
460 as well as to constrain the provenance of an unknown sample.
461
462 This study analyzed museum-quality specimens; further work is needed on weathered and
463 recycled samples, which are commonly encountered in forensic evidence, to ensure they behave
464 similarly. Replicate measurements on the same sample have shown excellent reproducibility for
465 the luminescence peak centroids, whereas measurements of different samples from around the
466 U.S. showed significant variability in the measured spectra. The intra-source spectral
467 homogeneity combined with inter-source diversity allows for source attribution of the samples in
468 this study. Of course, much larger libraries of spectra are necessary to use luminescence

spectroscopy routinely as a guide for provenance. However, even without large spectral libraries, luminescence spectroscopy may still be useful as an additional forensic tool for the comparison of sediment samples.

ACKNOWLEDGMENTS

This work was funded by the National Science Foundation (RUI PHY-0969058; MRI 0319523), and Department of Homeland Security (2008-DN-077-ER0008) and the FBI Laboratory Division. This research was supported in part by an appointment to the Visiting Scientist Program at the FBI Laboratory Division, administered by Oak Ridge Institute for Science and Education, through an interagency agreement between the U.S. Department of Energy and the Federal Bureau of Investigation, and Hope College Chemistry and Physics Departments. We thank the Smithsonian Institution National Museum of Natural History Department of Mineral Sciences for samples and Paul Pohwat, Dave Daugherty, Edward Hansen, Jonathan Peterson, Joshua Borycz, Alyssa Cassabaum, and Robert Koons for their contributions.

This is publication number 13-08 of the Laboratory Division of the Federal Bureau of Investigation (FBI). Names of commercial manufacturers are provided for information only and inclusion does not imply endorsement by the FBI. Points of view in this document are those of the authors and do not necessarily represent the official position of the FBI or the U.S. Government.

492

493

REFERENCES CITED

Armstrong, J.T. (1988) Quantitative analysis of silicate and oxide materials: comparison of Monte Carlo, ZAF, and phi-rho-z procedures. Microbeam Analysis, 239-246.

Bernard, J.H. and Hyršl, J. (2004) Minerals and their Localities, 823p. Granit, s.r.o., Czech Republic.

Berry, L.G., Ed. (1974) Selected Powder Diffraction Data for Minerals: Data Book, First Ed. Joint Committee on Powder Diffraction Standards, Swarthmore, PA.

Bowen, A.M. and Caven, E.A. (2013) Forensic provenance investigations of soil and sediment samples. In D. Pirrie, A. Ruffell, and L.A. Dawson, Eds., Environmental and Criminal Geoforensics, Geological Society, London, Special Publications, 384, 9-25.

Correcher, V. and Garcia-Guinea, J. (2001) On the luminescent properties of adularia feldspar. Journal of Luminescence, 93, 303-312.

Deer, W.A., Howie, R.A., and Zussman, J. (1966) An Introduction to the Rock Forming Minerals, p. 282-338. Longman Group Limited, London.

Erfurt, G. (2003) Infrared luminescence of Pb^{+} centres in potassium-rich feldspars. Physica Status Solidi (A), 200, 429-438.

Erfurt, G. and Krbetschek, M.R. (2003) Studies on the physics of the infrared radioluminescence of potassium feldspar and on the methodology of its application to sediment dating. Radiation Measurements, 37, 505-510.

Finch, A.A. and Klein, J. (1999) The causes and petrological significance of cathodoluminescence emissions from alkali feldspars. Contributions to Mineralogy and Petrology, 135, 234-243.

Finch, A.A., Hole, D.E., and Townsend, P.D. (2003) Orientation dependence of luminescence in plagioclase. Physics and Chemistry of Minerals, 30, 373-381.

Fockele, M., Lohse, F., Spaeth, J-M., and Bartram, R.H. (1989) Identification and optical properties of axial lead centres in alkaline-earth fluorides. Journal of Physics: Condensed Matter, 1, 13-26.

Garcia-Guinea, J., Finch, A., Can, N., Hole, D., and Townsend, P. (2007) Orientation dependence of the ion beam and cathodoluminescence of albite. Physica Status Solidi (C), 4, 910-913.

Gorobets, B.S. and Rogojine, A.A. (2002) Luminescent Spectra of Minerals: Reference Book, 300 p. All Russia Institute of Mineral Resources (VIMS), Moscow.

Götze, J. (2000) Cathodoluminescence in applied geosciences. In M. Pagel, V. Barbin, P. Blanc, D. Ohnenstetter, Eds., Cathodoluminescence in the Geosciences, p. 457-477. Springer-Verlag, Berlin.

Götze, J. (2002) Potential of cathodoluminescence microscopy and spectroscopy for the analysis of minerals and materials. Analytical and Bioanalytical Chemistry, 374, 703-708.

Götze, J., Haberman, D., Neuser, R.D., and Richter D.K. (1999) High resolution spectrometric analysis of rare earth elements-activated cathodoluminescence in feldspar minerals. Chemical Geology, 153, 81-91.

Götze, J., Krbetschek, M.R., Habermann D., Wolf, D. (2000) High resolution cathodoluminescence studies of feldspar minerals. In M. Pagel, V. Barbin, P. Blanc, and D. Ohnenstetter, Eds., Cathodoluminescence in the Geosciences, p. 245-270. Springer-Verlag, Berlin.

Gütlich, P., Hauser, A., Spiering, H. (1994) Thermal and optical switching of Iron (II) complexes. Angewandte Chemie, 33, 2024-2054.

Haberman, D. (2002) Quantitative cathodoluminescence (CL) spectroscopy of minerals: Possibilities and limitations. Mineralogy and Petrology, 76, 247-259.

Hofmeister, A.M. and Rossman, G.R. (1985) Exsolution of metallic copper from Lake County Labradorite. Geology, 13, 644-647.

Johnston, C.L., Gunter, M.E., and Knowles, C.R. (1992) Sunstone Labradorite from the Ponderosa Mine, Oregon. Gems and Geology, 27, 220-233.

Kabler, M.N. (1964) Low temperature recombination luminescence in alkali halide crystals. Physical Review, 136, A1296–A1302.

Krbetschek, M.R., Götze, J., Irmer, G., Rieser, U., and Trautman, T. (2002) The red luminescence emission of feldspar and its wavelength dependence on K, Na, Ca – composition. Mineralogy and Petrology, 76, 167-177.

Latkoczy, C., Ducking, M., Becker, S., Gunther, D., Hoogewerff, J., Almirall, J., Buscaglia, J., Dobney, A., Koons, R., Montero, S., van der Peijl, G.J.Q., Stoecklein, W., Trejos, T., Watling, J., and Zdanowicz, V. (2005) Development and evaluation of a standard method for the quantitative determination of elements in float glass samples by LA-ICP-MS. Journal of Forensic Sciences, 50, 1327-1341.

Maxwell, J.A., Teesdale, W.J., Campbell, J.L. (1995) The Guelph PIXE software package II. Nuclear Instruments and Methods in Physics Research Section B: Beam Interactions with Materials and Atoms, 95, 407–421.

584 Mora, C.I. and Ramseyer, K. (1992) Cathodoluminescence of coexisting plagioclases, Boehls
585 Butte anorthosite: CL activators and fluid flow paths. American Mineralogist, 77, 1258–
586 1265.
587
588 Morgan, R.M. and Bull, P.A. (2007) The philosophy, nature and practice of forensic sediment
589 analysis. Progress in Physical Geography, 31(1), 43-58.
590
591 Munisso, M.C., Zhu, W., Leto, A., and Pezzotti, G. (2007) Stress dependence of sapphire
592 cathodoluminescence from optically active oxygen defects as a function of crystallographic
593 orientation. Journal of Physical Chemistry A, 111, 3526-3533.
594
595 Nagli, L.E. and Dyachenko, S.V. (1988) Influence of a v_e^- vacancy on luminescence of Pb^+
596 centres in alkali halides. Physica Status Solidi (C), 146, 295-301.
597
598 Palenik, C.S. and Buscaglia, J. (2007) Applications of cathodoluminescence in forensic science.
599 In R.D. Blackledge, Ed., Forensic Analysis on the Cutting Edge: New Methods for Trace
600 Evidence Analysis, p. 141-172. John Wiley & Sons Inc., New York.
601
602 Parsons, I., Steele, D.A., Lee, M.R., and Magee, C.W. (2008) Titanium as a
603 cathodoluminescence activator in alkali feldspars. American Mineralogist, 93, 875-879.
604
605 Petraco, N., Kubic, T.A., and Petraco, N.D.K. (2008) Case studies in forensic soil examinations.
606 Forensic Science International, 178, e23-e27.
607
608 Pye, K. and Blott, S.J. (2009) Development of a searchable major trace element database for use
609 in forensic soil comparisons. Science and Justice, 49, 170-181.
610
611 Pye, K. and Croft, D.J. (2004) Forensic geoscience: Introduction and overview. In K. Pye and
612 D.J. Croft, Eds. Forensic Geoscience: Principles, Techniques and Applications. Geological
613 Society, London, Special Publications, 232, 1-5.
614
615 Ralchenko, Y., Kramida, A.E., Reader, J., and NIST ASD Team (2011). NIST Atomic Spectra
616 Database (ver. 4.1.0), [Online]. Available: http://physics.nist.gov/asd [2012, February 15].
617 National Institute of Standards and Technology, Gaithersburg, MD.
618
619 Reader, J., Corliss, C.H., Wiese, W.L., and Martin, G.A. (1980). Wavelengths and transition
620 probabilities for atoms and atomic ions, part I. Wavelengths, part II. Transition
621 Probabilities, National Standard Reference Data Series, NSRDS-NBS 68, 415p. U.S.
622 Government Printing Office, Washington, D.C.
623
624 Rendell, H.M. and Clarke, M.L. (1997) Thermoluminescence, radioluminescence, and
625 cathodoluminescence spectra of alkali feldspars. Radiation Measurements, 27, 263-272.
626
627 Ribbe, P.H. (1975) The chemistry, structure, and nomenclature of feldspars. In P. H. Ribbe,
628 Eds., Short Course Notes, Feldspar Mineralogy, vol. 2, p. 1-72. Mineralogical Society of
629 America.

Ruffell, A. and McKinley, J. (2005) Forensic geoscience: Applications of geology, geomorphology and geophysics to criminal investigations. Earth-Science Reviews, 69, 235-247.

Telfer, D.J. and Walker, G. (1978) Ligand field bands of Mn^{2+} and Fe^{3+} luminescence centres and their site occupancy in plagioclase feldspars. Modern Geology, 6, 199-210.

Thomas, J.K. (1987) Characterization of surfaces by excited states. The Journal of Physical Chemistry, 91, 267-276.

Walderhaug, O. and Rykkje J. (2000) Some examples of the effect of crystallographic orientation on the cathodoluminescence colors of quartz. Journal of Sedimentary Research, 70, 545-548.

FIGURE CAPTIONS

Figure 1. Ternary plot of feldspar major elemental composition based on μXRF data for percent orthoclase (Or) for $KAlSi_3O_8$ component (where %Or = K/K+Ca+Na), albite (Ab) for $NaAlSi_3O_8$ component (where %Ab = Na/K+Ca+Na), and anorthite (An) for $CaAl_2Si_2O_8$ component (where %An = Ca/K+Ca+Na), by mole fraction. Calculated error on these compositions can be found in Appendix 1.

Figure 2. Chemical composition (computed as mol %Ca of Ca+Na+K) results for plagioclase feldspar samples from the Ward's Science Reference Series, as determined by three analytical techniques used in this study.

Figure 3. Representative CL feldspar spectra. The luminescence intensity is measured in arbitrary units (A.U.). The individual curves for each mineral type represent spectra collected from six replicate mineral grains from the same source. (a) Microcline from Barringer Hill, Texas (F2, Appendix 1); (b) Oligoclase from Bakersville, North Carolina (F28, Appendix 1); and (c) Labradorite from Lake County, Oregon (F31, Appendix 1). The spectra were smoothed for clarity. Statistical error bars are not shown on the individual spectra, because the error associated with channel-to-channel fluctuations in the individual data points are smaller than ~3% and do not appear distinctly when plotted.

Figure 4. Examples of CL spectral variability among feldspars as a function of geographical provenance. The luminescence intensity is measured in arbitrary units (A.U.). While the mineral composition does not change for these alkali (a) or Ca-rich plagioclase (greater than 50%

668 Anorthite) feldspars (b), subtle trace elemental substitutions within each sample leads to obvious
669 CL peak shifts between various feldspar samples from different geographic origins. All spectra
670 have been smoothed for clarity. Statistical error bars are not shown on the individual spectra,
671 because the error associated with channel-to-channel fluctuations in the individual data points are
672 smaller than ~5% and do not appear distinctly when plotted.

673 Note: Based on the variability in chemical composition within a sample, samples from each
674 mineral location are given a general feldspar classification.
675

676 **Figure 5**. Observed d-spacing by XRD for the (002) plane compared to CL peak centroid
677 wavelengths measured for the Fe^{3+} peak in a variety of feldspar samples. Only samples with Fe
678 peaks comprising more than 10% of the total CL spectrum were included in this analysis. Error
679 bars reflect averages from greater than three manual fittings of the spectra to account for the
680 variations that can occur when manually deconvolving spectra.
681

682 **Figure 6.** Representative IBIL and CL spectra of a well-studied zircon. The luminescence
683 intensity is measured in arbitrary units (A.U.). Regardless of luminescence technique (CL or
684 IBIL), REE peak centroids are consistent within analytical error of ±4 nm between the two
685 measurement techniques.
686

687 **Figure 7.** Representative IBIL and CL spectra of the F31 feldspar sample. The luminescence
688 intensity is measured in arbitrary units (A.U.). When observing a representative feldspar sample
689 from this study (F31, Appendix 1), there were excitation technique-dependent inconsistencies in
690 these features: blue (~400 nm Cu^{2+}) and red (~670-750 nm Fe^{3+}) peak positions reflected a

hypsochromic and a bathochromic shift, respectively, in the IBIL spectra when compared with the CL spectra.

TABLE CAPTIONS

Table 1. Numerical peak centroid positions from the CL spectra included in Fig. 4, with corresponding full-width at half-maximum (FWHM) and standard deviation (error) for six replicate measurements. Peaks not detected in a sample are indicated by (-) for each value. Based on the variability in chemical composition within a sample, samples from each mineral location are given a general feldspar classification. Samples are identified fully in Appendix 1 by the sample number in parentheses.

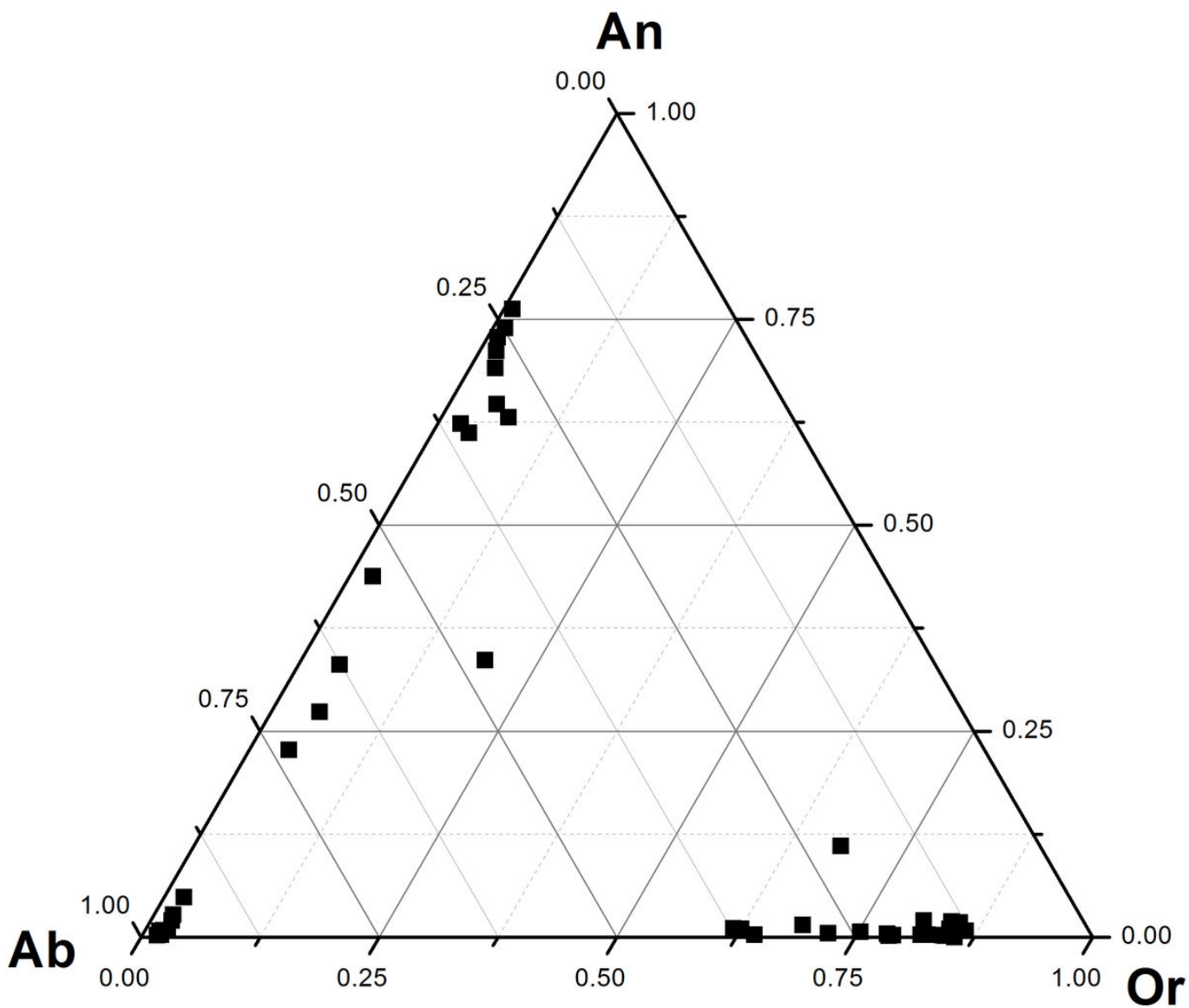
An
0.00
1.00
0.25
0.75
0.50
0.50
0.75
0.25
1.00
0.00
Ab
0.00
0.25
0.50
0.75
1.00
Or

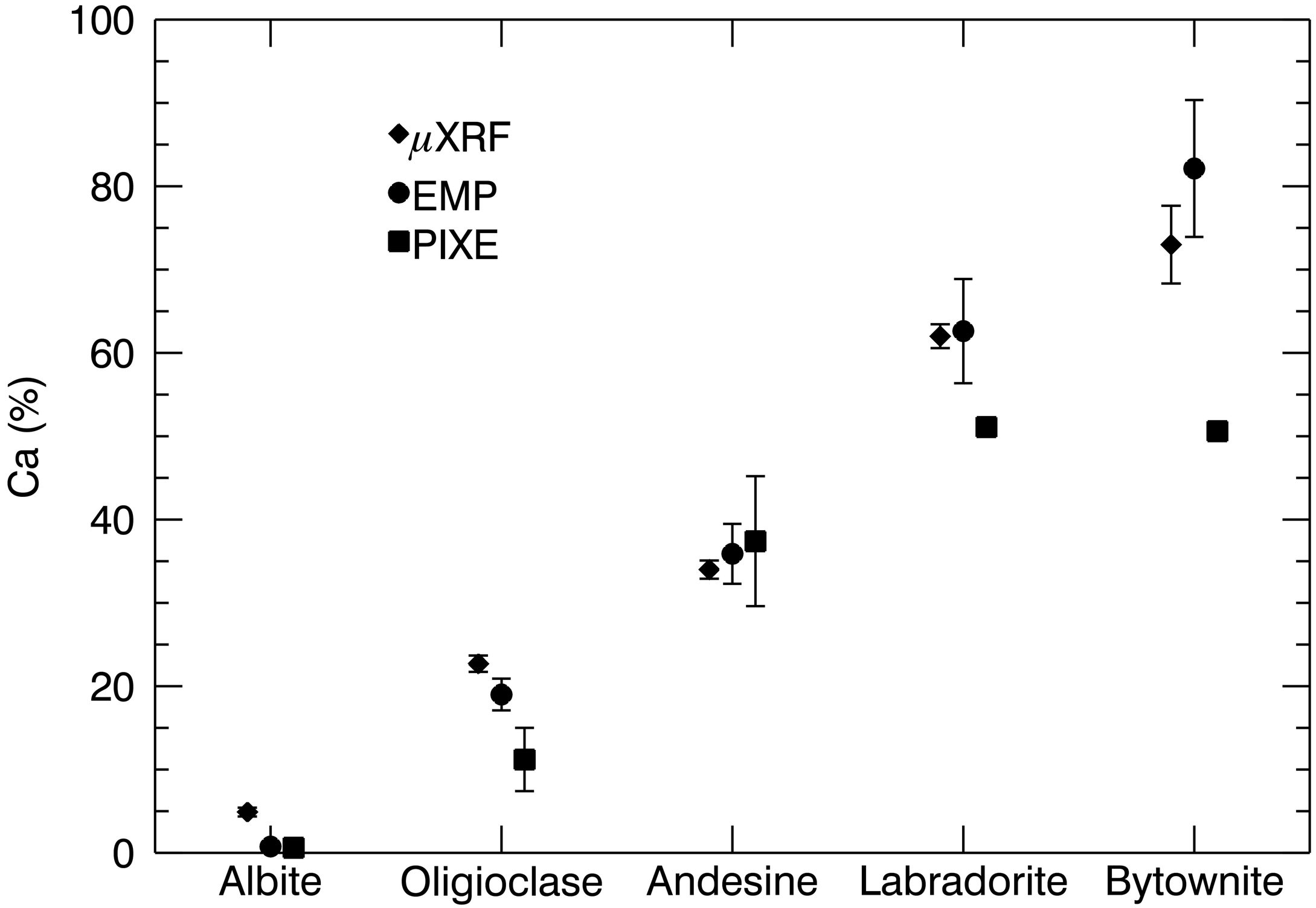
100
80
60
40
20
0
Ca (%)
μXRF
EMP
PIXE
Albite
Oligioclase
Andesine
Labradorite
Bytownite

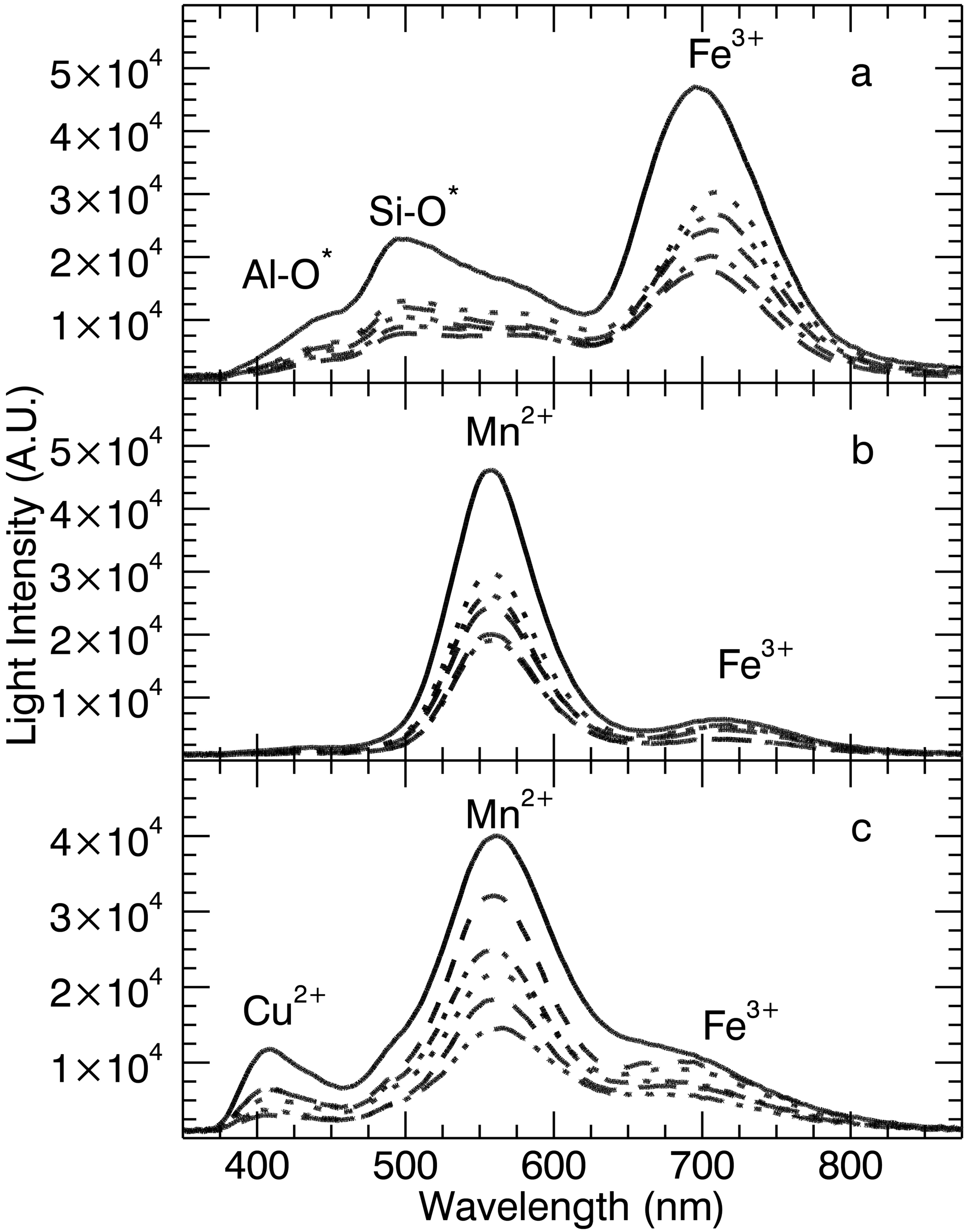
Fe3+
a
Si-O*
Al-O*
5×10^4
4×10^4
3×10^4
2×10^4
1×10^4
Mn2+
b
Fe3+
Light Intensity (A.U.)
Mn2+
c
Cu2+
Fe3+
400
500
600
700
800
Wavelength (nm)

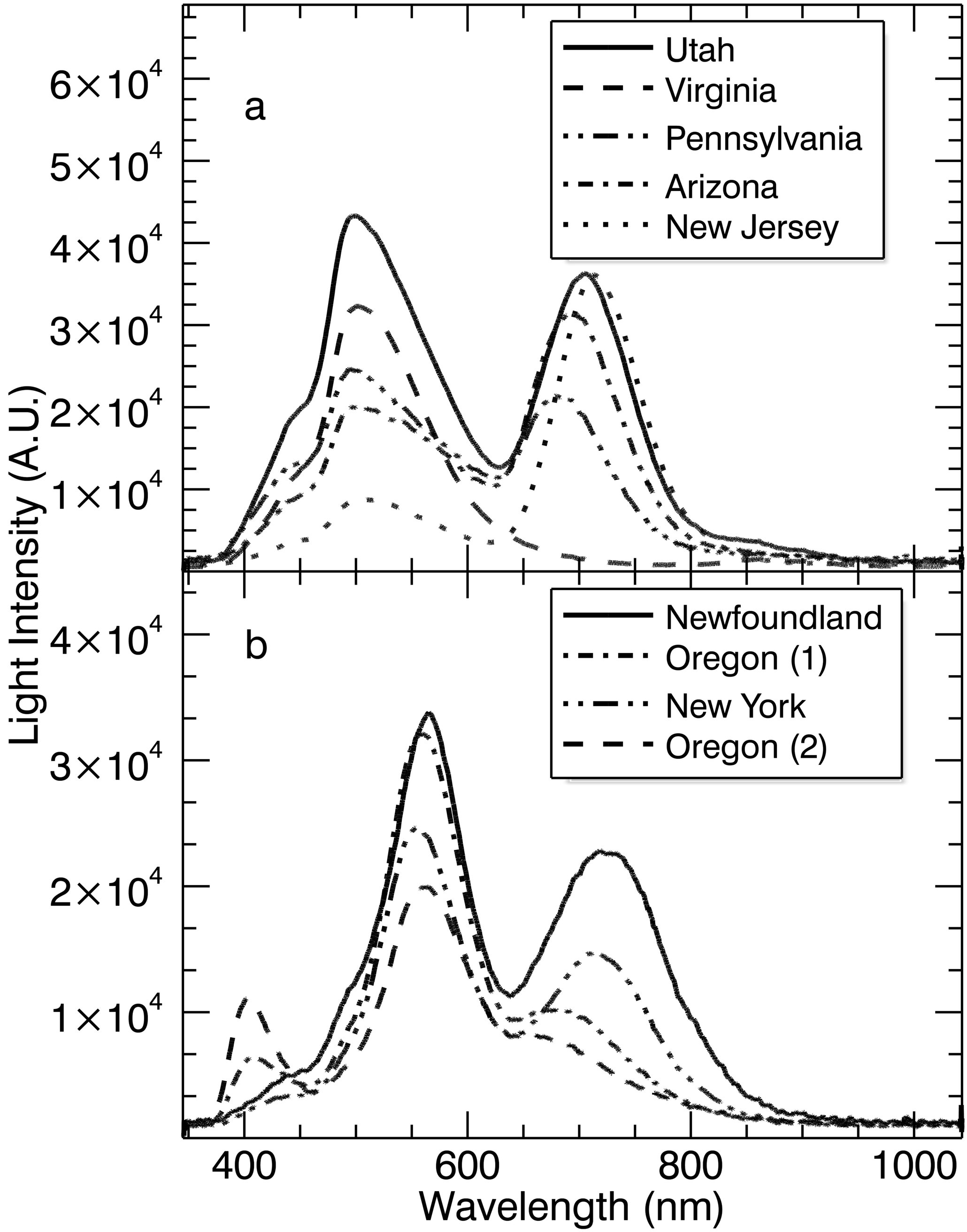
a
b
Utah
Virginia
Pennsylvania
Arizona
New Jersey
Newfoundland
Oregon (1)
New York
Oregon (2)
Light Intensity (A.U.)
6×10^4
5×10^4
4×10^4
3×10^4
2×10^4
1×10^4
4×10^4
3×10^4
2×10^4
1×10^4
400
600
800
1000
Wavelength (nm)

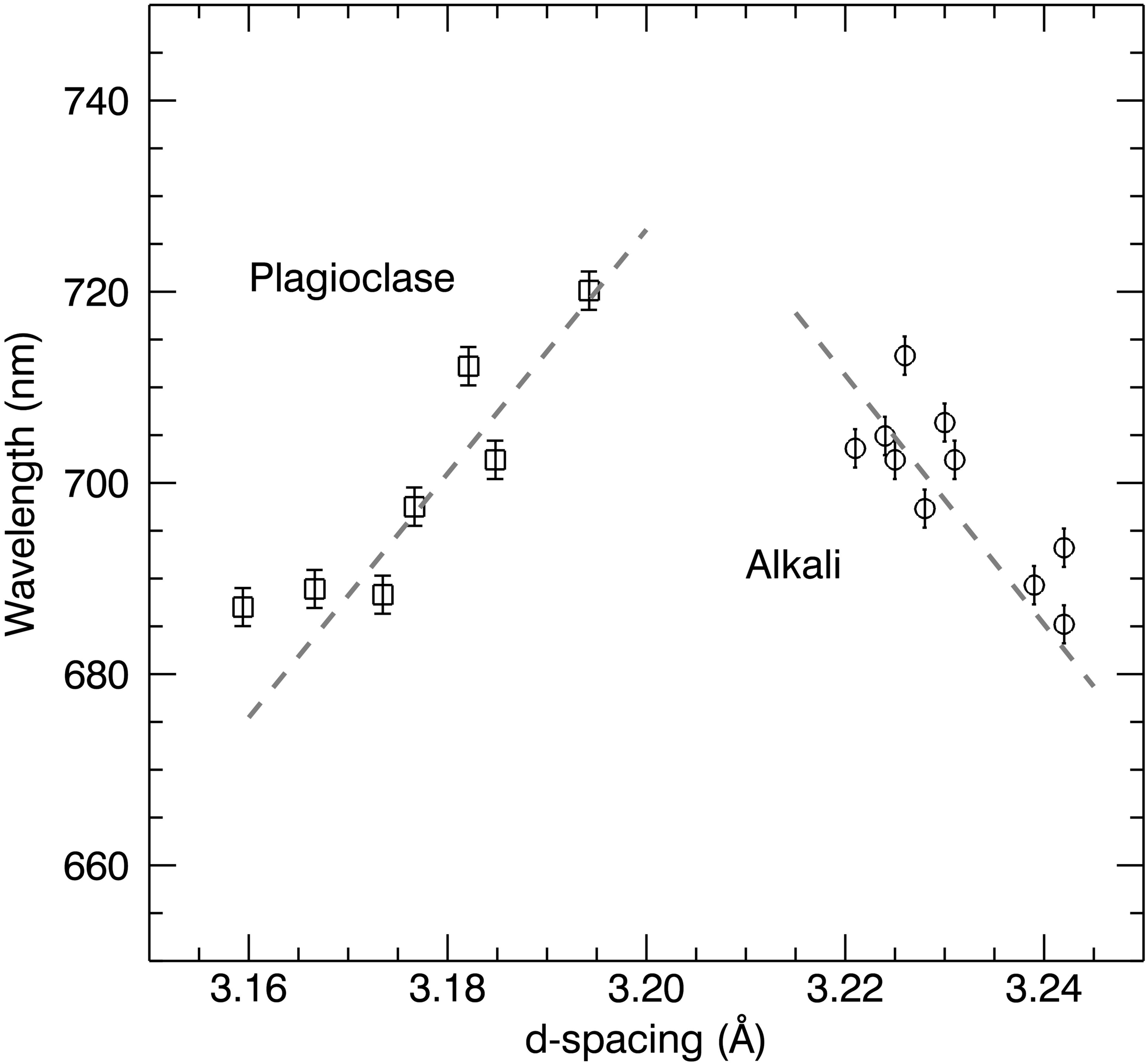
740
720
700
680
660
Wavelength (nm)
Plagioclase
Alkali
3.16
3.18
3.20
3.22
3.24
d-spacing (Å)

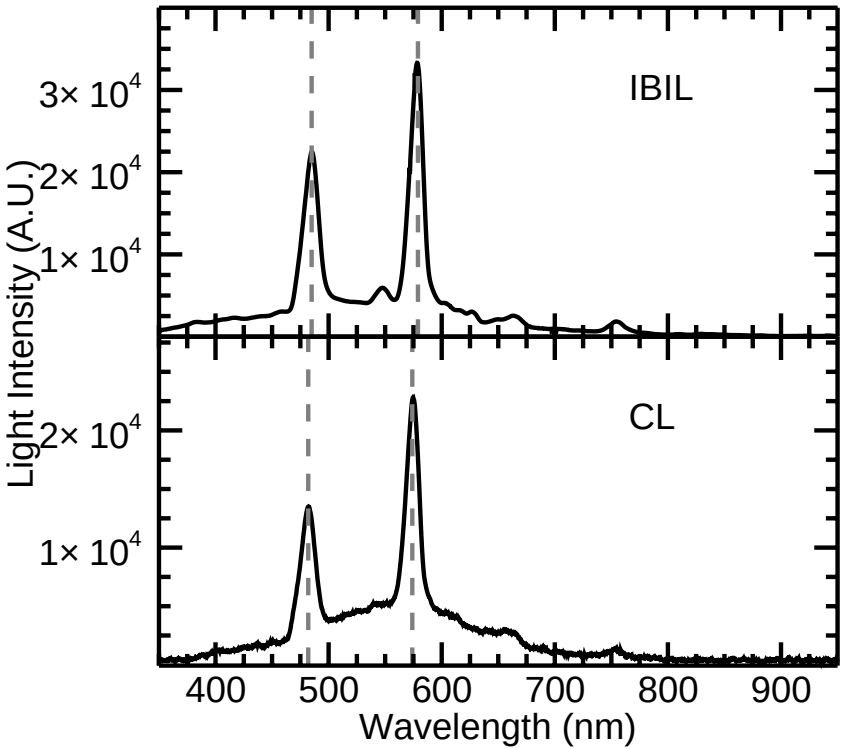
IBIL
CL
Light Intensity (A.U.)
3× 10^4
2× 10^4
1× 10^4
2× 10^4
1× 10^4
400
500
600
700
800
900
Wavelength (nm)

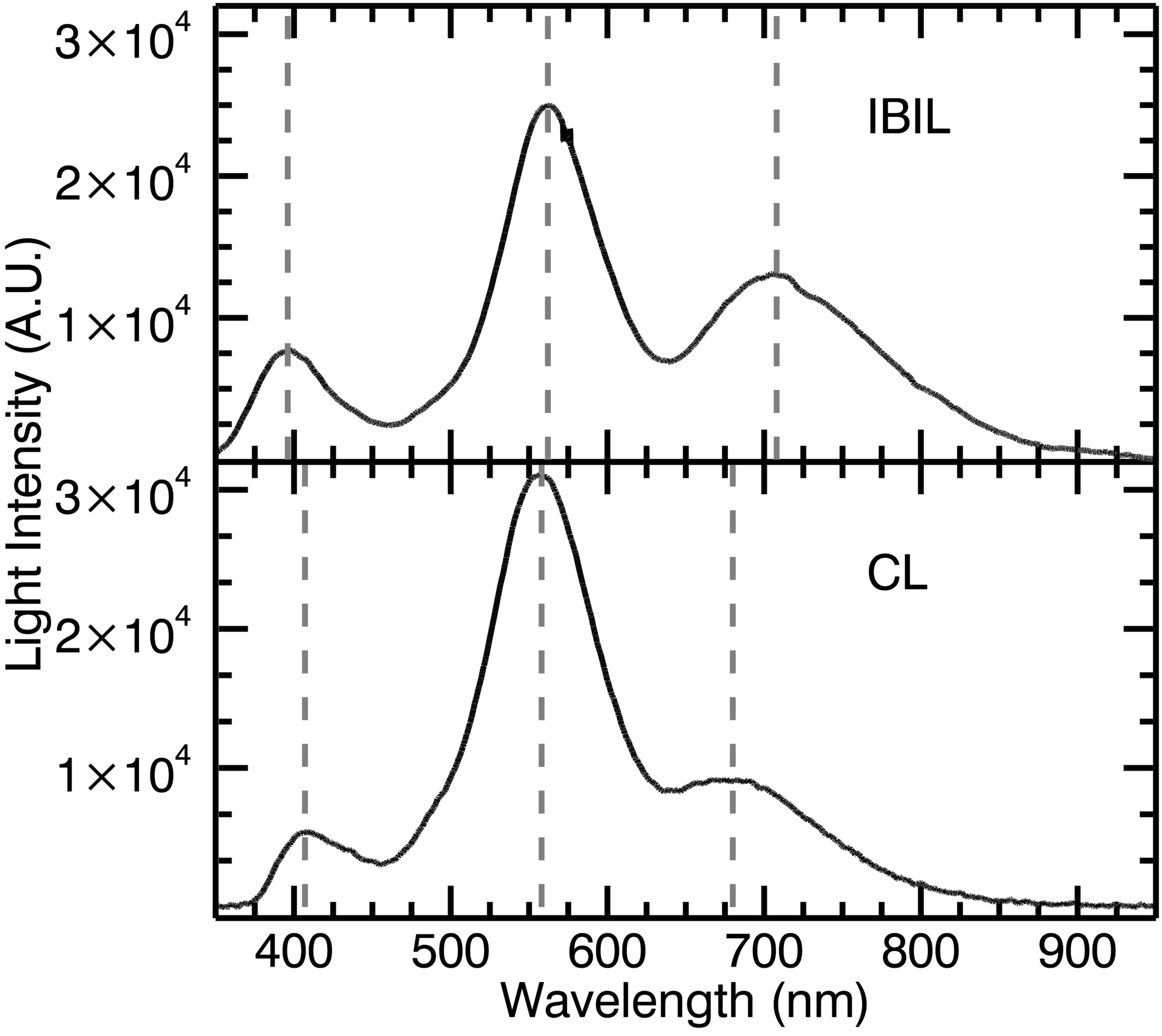
3×10^4
2×10^4
1×10^4
IBIL
3×10^4
2×10^4
1×10^4
CL
Light Intensity (A.U.)
400
500
600
700
800
900
Wavelength (nm)

Mineral Location		Fe^{3+} Peak Centroids (nm)	FWHM (nm)
Alkali			
Utah	(F4)	697(6)	45
Virginia	(F1)	-	-
Pennsylvania	(F11)	707(8)	78
Arizona	(F9)	685(1)	79
New Jersey	(F13)	713(7)	78
Plagioclase (Ca-rich)			
Newfoundland	(F30)	720(4)	109
Oregon (1)	(F31)	688(4)	106
Oregon (2)	(F34)	678(4)	105
New York	(F36)	712(2)	99